ACCSCIENCE PUBLISHING

Asian Journal of Water, Environment and Pollution

ORIGINAL RESEARCH ARTICLE

Spatial dynamics of river salinity and vegetation cover in the Tigris–Euphrates Basin, Iraq

Afrah L. Mohammed Rasheed, Raghad Mouhamad*, Khanssaa M. Abdulmajed, and Shrooq R. Hameed

Scientific Research Commission, Baghdad, Iraq

Abstract

Water scarcity in the Tigris–Euphrates basin is increasingly accompanied by deteriorating irrigation-water salinity and strong spatial contrasts in land cover. This study evaluates river-salinity gradients together with Landsat-derived vegetation-cover patterns using four 2021 monitoring campaigns (March, April, June, and July), exact WGS 84 coordinates for 18 Tigris and 14 Euphrates locations, irrigation water quality index (IWQI) scores, and distance-based repeated-measures models. The updated coordinate–electrical conductivity (EC) workbooks contained 125 non-missing EC observations, all of which matched the quality-controlled analytical archive. Cumulative inter-station geodesic distance was 897.48 km for the Tigris monitoring sequence and 779.16 km for the Euphrates sequence. Mean EC was 1.08 ± 0.65 dS/m in the Tigris and 1.55 ± 1.06 dS/m in the Euphrates; mean IWQI was 87.78 ± 8.60 and 82.53 ± 15.47, respectively. Linear mixed-effects models with station random intercepts and campaign fixed effects estimated EC increases of 0.217 dS/m per 100 km in the Tigris (95% confidence interval: 0.174–0.259) and 0.385 dS/m per 100 km in the Euphrates (0.251–0.520), with corresponding IWQI declines of 2.79 and 5.60 units per 100 km (all $p < 0.001$). The Euphrates distance slope was significantly steeper for EC, total dissolved solids, and IWQI (river × distance $p = 0.007$, 0.004, and 0.002, respectively). First-order autoregressive correlation generalized estimating equations, leave-one-station-out analyses, omission of the three lower-Euphrates April gaps, exclusion of the disputed Al-Baghdadi IWQI value, and removal of Al-Madina independently preserved the downstream signal. Both marginal and conditional first-neighbor residual Moran tests showed no evidence of remaining longitudinal autocorrelation after false-discovery rate control. Landsat-derived normalized difference vegetation index mapped the basin-scale summer vegetation-cover pattern, whereas the optical salinity index was retained as environmental context rather than treated as a calibrated predictor of river chemistry. The results identify the lower Tigris and, more specifically, the Shinafiyah–Al-Madina sector of the Euphrates as priority reaches for salinity surveillance and adaptive irrigation-water management.

Keywords: Tigris River; Euphrates River; Electrical conductivity; Irrigation water quality index; Geodesic distance; Normalized difference vegetation index; Landsat 8; Mixed-effects model

***Corresponding author:**
Raghad Mouhamad
(Raghad.s.mouhamad@src.edu.iq)

Citation: Rasheed ALM, Mouhamad R, Abdulmajed KM, Hameed SR. Spatial dynamics of river salinity and vegetation cover in the Tigris–Euphrates Basin, Iraq. *Asian J Water Environ Pollut.* doi: 10.36922/AJWEP026340239

Received: August 20, 2026

Revised: September 4, 2026

Accepted: September 10, 2026

Published online: September 21, 2026

Copyright: © 2026 Author(s). This is an Open-Access article distributed under the terms of the Creative Commons Attribution License, permitting distribution, and reproduction in any medium, provided the original work is properly cited.

Publisher's Note: AccScience Publishing remains neutral with regard to jurisdictional claims in published maps and institutional affiliations.

1. Introduction

Water security is no longer defined only by the quantity of water available to a basin; the quality of that water and its suitability for productive use are equally decisive. Cross-country analyses show that water security is linked to broader socio-economic performance, while recent basin studies increasingly treat hydrological availability, irrigation demand, and water quality as interacting components rather than separate problems.[1] A strong example is the Tigris–Euphrates River basin. Satellite observations and hydro-climate data analysis show a significant reduction in downstream water availability due to climate variability, evaporation, reservoir storage, and increased human water use.[2] Flow regimes have also shown the effect of upstream development in the Iraqi part of the Tigris River basin,[3] while water accounting studies in the basin show poor irrigation efficiency on farms and increased water consumption.[4] These factors increase the chances of saline water being used for irrigation in the Mesopotamian plain.[5]

Reduced freshwater influx, evaporation, return flow, and hydraulic control have historically been linked to downstream mineralization in Iraq.[6,7] Research on the Tigris has shown increased salinity and dissolved loads at downstream sections,[8,9] while studies on the Euphrates have identified spatial degradation from the middle to lower parts of the river.[10,11] A 2026 study of the Tigris in Baghdad found that the river's quality was affected not only by natural hydrogeochemical factors but also by urban and agricultural impacts.[12] Studies on the western Euphrates have similarly shown geogenic and anthropogenic influence on water quality as well as river–aquifer relations.[13] However, direct comparison of the two rivers of Iraq within the same coordinate-resolved longitudinal repeated-measures design has rarely been undertaken.

Electrical conductivity (EC) and total dissolved solids (TDS) estimate salinity and the number of dissolved ions, respectively; however, no single index provides sufficient information on the multiple factors that constrain the agricultural applicability of water. The Iraqi irrigation water quality index (IWQI) was devised to synthesize information on salinity, permeability, toxicity of particular ions, toxicity of trace elements, and other aspects of water impacts on the most sensitive crops on a 0-to-100 scale.[14] Since then, the index has been implemented for the main Iraqi rivers using the IWQI software,[15] while the parameters have been defined based on the Food and Agriculture Organization irrigation water guidelines.[16] The transparency of the mathematical basis of water quality indices is important for complete comprehension, as in river–WQI studies outside Iraq.[17]

Geospatial data adds another layer to irrigation water evaluation. Remote sensing has a well-established history for characterizing saline soils and plant canopies or vegetation;[18-21] nevertheless, optical measurements are prone to interference from factors such as soil brightness, moisture content, land use, and plant development stage. Recent reviews highlight the need for explicit preprocessing, field calibration when quantitative soil salinity is claimed, and uncertainty analysis before applying remote sensing relations to water quality modeling.[22-24] In this study, exact station coordinates provide the quantitative spatial scale for river-salinity analysis, while Landsat normalized difference vegetation index (NDVI) is used to map basin-scale summer vegetation cover and an optical salinity index (SI) is retained as regional environmental context. Neither index is used as an uncalibrated predictor of river chemistry.

The study addresses four questions:

(i) How strongly do EC, TDS, and IWQI change along cumulative monitoring-sequence geodesic distance in the Tigris and Euphrates?
(ii) Does the rate of deterioration differ between rivers after repeated observations and campaign effects are accounted for?
(iii) Are the principal conclusions stable to temporal correlation, influential stations, downstream April missingness, and IWQI data-integrity decisions?
(iv) What basin-scale summer vegetation-cover and optical-salinity patterns are resolved by Landsat across the same Iraqi setting?

The analysis therefore couples coordinate-resolved river chemistry with a separately interpreted vegetation-cover map, avoiding causal satellite–hydrochemistry claims that are not supported by field calibration.

2. Materials and methods

2.1. Study area, monitoring network, and sampling design

The monitoring network covers the Iraqi courses of the Tigris and Euphrates from upstream entry reaches to Al-Qurnah. The updated station files provide WGS 84 geographic coordinates for 18 Tigris locations and 14 Euphrates locations (Figure 1). Water was sampled in March, April, June, and July 2021. The analytical unit was river × station × campaign. Missing observations remained missing; no zero substitution, mean imputation, or interpolation of hydrochemical values was used. The source monitoring program scheduled campaigns using operational hydrological information available at the time, but discharge was not retained as an observation-level

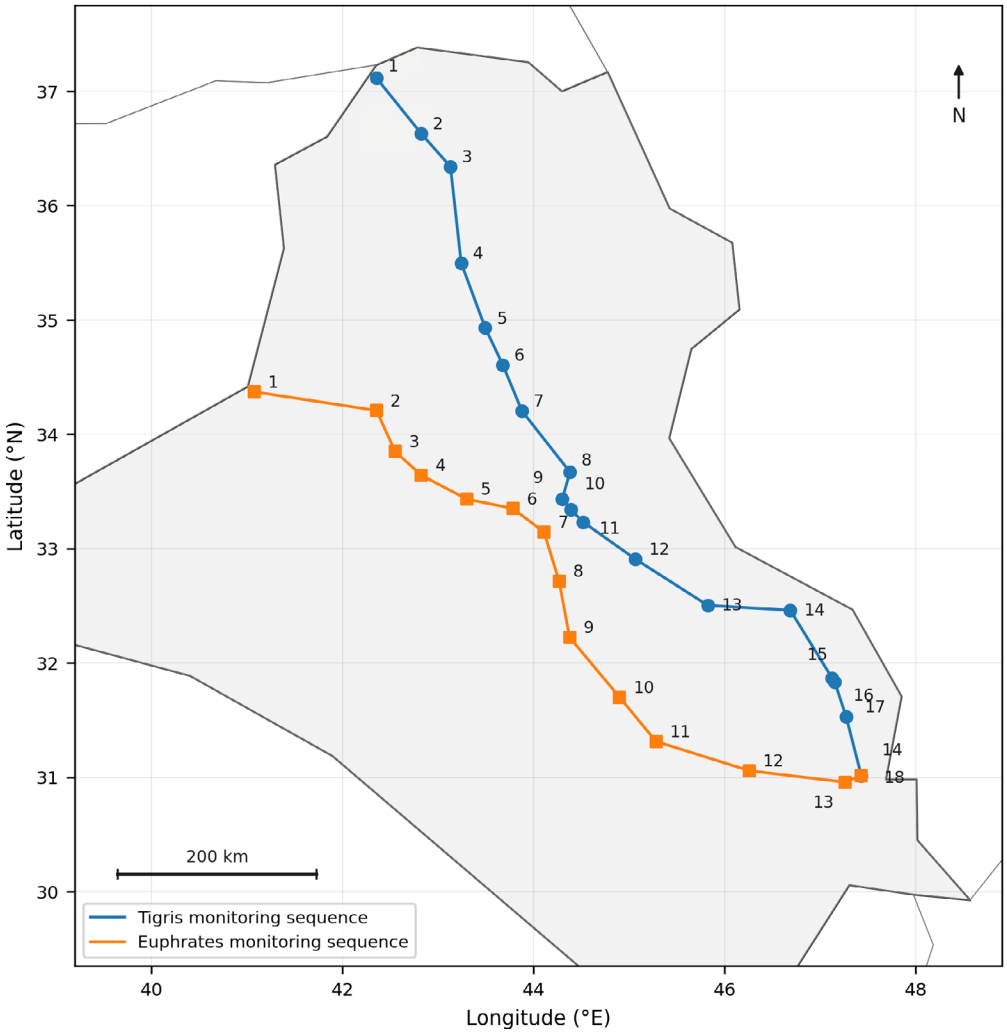


Figure 1. WGS 84 coordinate monitoring network revised for the 2021 Tigris–Euphrates campaigns. The numbers refer to the up-down sequence of the stations along each river. The lines connecting these numbers represent the sequence used to calculate the total geodesic distance; they do not represent the river centerline.

variable and was therefore not included as a covariate in the present models.

Data quality assurance was performed by validating the new coordinate–EC workbooks against the quality-controlled station month archive. There were perfect matches between all 72 Tigris EC observations and all 53 Euphrates EC observations (125/125). In addition, the new coordinate file for the Euphrates contains WGS 84 coordinates that eliminate ambiguity in terms of station locations in the 14-station series. Table 1 provides information on the monitoring geometry, cumulative distances, EC readings, and observations used in the analysis.

2.2. Hydrochemical measurements and analytical quality control

Electrical conductivity measurements were made at 25 °C. TDS were measured independently in the laboratory rather than derived from EC values. Calcium and magnesium were measured using ethylenediaminetetraacetic acid titration, and sodium was determined through flame photometry in the source program. This methodological distinction matters because the relationship between EC and TDS is empirical, not a fixed conversion ratio. The source documentation contains information on instrument calibration, duplication, blank confirmation, and range check. Instrument-specific detection limits and duplicate error reports were not included in the analytical

Table 1. Monitoring network, updated WGS 84 coordinates, cumulative inter-station geodesic distance, campaign EC values, and retained observation counts

River	Rank	Station	Latitude	Longitude	Cum. km	March EC	April EC	June EC	July EC	IWQI *n*
Tigris	1	Feshkhabur	37.1156	42.3556	0.0	0.45	0.42	0.35	0.36	4
Tigris	2	Mosul Dam	36.6295	42.8239	68.2	0.45	0.45	0.36	0.38	4
Tigris	3	Mosul	36.3400	43.1300	110.5	0.50	0.45	0.40	0.50	4
Tigris	4	Shirqat	35.4983	43.2422	204.6	0.49	0.42	0.44	0.52	4
Tigris	5	Baiji	34.9306	43.4939	271.8	0.52	0.41	0.44	0.50	4
Tigris	6	Tikrit	34.6064	43.6783	311.6	0.51	0.43	0.46	0.49	4
Tigris	7	Samarra Barrage	34.2047	43.8775	359.8	0.54	0.42	0.48	0.48	4
Tigris	8	Tarmiyah	33.6694	44.3806	435.3	0.54	0.43	0.52	0.54	2
Tigris	9	Tharthar Arm	33.4333	44.3000	462.6	1.16	1.51	1.63	1.71	2
Tigris	10	Baghdad Sarai	33.3403	44.3897	475.9	0.61	1.10	1.02	1.28	4
Tigris	11	Tigris-Diyala Confluence	33.2325	44.5186	492.8	0.82	1.12	1.10	1.24	4
Tigris	12	Aziziyah	32.9103	45.0622	554.9	1.14	1.13	1.24	1.32	4
Tigris	13	Kut	32.5036	45.8233	639.2	1.23	1.16	1.24	1.48	4
Tigris	14	Ali Al-Gharbi	32.4608	46.6869	720.4	1.76	2.00	1.66	1.60	4
Tigris	15	Branching Regulators	31.8681	47.1242	798.1	1.98	2.08	1.64	1.72	4
Tigris	16	Amarah Barrage	31.8347	47.1519	802.6	2.08	2.10	1.70	1.79	4
Tigris	17	Qalat Saleh	31.5286	47.2717	838.5	2.37	2.13	1.80	1.79	4
Tigris	18	Al-Qurnah	31.0156	47.4300	897.5	2.39	2.34	1.83	1.85	4
Euphrates	1	Al-Qaim	34.3708	41.0772	0.0	0.69	0.80	1.24	1.08	3
Euphrates	2	Haditha Dam	34.2081	42.3556	118.8	0.80	0.78	0.75	0.78	4
Euphrates	3	Al-Baghdadi	33.8502	42.5502	162.5	0.81	0.81	0.78	0.80	4
Euphrates	4	Hit	33.6417	42.8250	196.9	0.84	0.84	0.83	0.85	4
Euphrates	5	Ramadi	33.4333	43.3000	246.6	0.92	0.92	0.86	0.88	4
Euphrates	6	Fallujah	33.3500	43.7833	292.4	0.93	0.97	1.10	1.15	4
Euphrates	7	Yusufiyah Head	33.1444	44.1086	330.4	1.10	1.00	1.13	1.16	4
Euphrates	8	Hindiya Barrage	32.7167	44.2667	380.2	1.02	1.03	1.08	1.18	4
Euphrates	9	Kifl	32.2242	44.3767	435.9	1.08	1.14	1.09	1.17	4
Euphrates	10	Shinafiyah	31.7000	44.9000	512.3	2.70	2.10	1.48	1.53	4
Euphrates	11	Samawah	31.3142	45.2811	568.4	2.90	–	2.06	2.14	3
Euphrates	12	Nasiriyah	31.0579	46.2572	665.5	3.85	–	3.21	3.37	3
Euphrates	13	Al-Madina	30.9575	47.2611	761.8	5.70	–	3.54	3.62	3
Euphrates	14	Al-Qurnah	31.0156	47.4300	779.2	3.10	2.45	1.92	1.98	4

Note: EC in dS/m. Cum. km is the cumulative sum of WGS 84 great-circle distances between successive monitoring locations and represents monitoring-sequence distance, not hydraulic channel chainage. – indicates campaigns for which no station observation was available. IWQI *n* is the number of retained IWQI observations across the four campaigns.
Abbreviations: EC: Electrical conductivity; IWQI: irrigation water quality index.

export and could not be reconstructed.

The quality-controlled analytical core retained 72 EC/TDS observations for the Tigris and 53 for the Euphrates. Major-cation observations were used as supporting hydrochemical evidence rather than as repeated-measures model responses. Across retained campaign summaries, Ca^{2+} ranged from 28 to 280 mg/L in the Tigris and from 35 to 220 mg/L in the Euphrates. Sodium reached 310 mg/L in the Tigris and 760 mg/L in the Euphrates, the latter occurring in the lower-river March record. These patterns are consistent with progressive downstream ionic enrichment documented in recent Iraqi river studies.[8-13]

Two IWQI observations required specific consideration regarding data integrity. The July Al-Qaim value of 912.86 falls outside the theoretical 0–100 scale and was therefore treated as invalid. The April Al-Baghdadi value of 61.93, although discordant with adjacent observations and with the station's EC/TDS pattern, remains within the valid IWQI scale and was retained in the primary analysis. A sensitivity analysis excluding 61.93 was used to determine whether the estimated IWQI gradient depended on this single observation.

2.3. Irrigation water quality index

Archived IWQI ratings were computed using the Iraqi methodology suggested by Al-Meini[14] and applied to major Iraqi rivers by Saloom & Oleiwi.[15] This approach assigns heterogeneous restrictions to the same 0–100 scale, where higher numbers represent less restrictive conditions. It organizes variables into five ordered groups: salinity; infiltration/permeability; specific-ion toxicity; trace-element toxicity; and miscellaneous effects on sensitive crops. Food and Agriculture Organization irrigation-water criteria provide the underlying agronomic interpretation[16] (**Equation 1**):

$$r_q = f_q(x_q), \quad 0 \le r_q \le 100 \tag{1}$$

For EC (x, dS/m), the published rating function was piecewise: $r_{EC} = 100$ for $x < 0.7$; $r_{EC}=113.13 - 18.75x$ for $0.7 \le x \le 1.5$; $r_{EC} = 110 - 16.667x$ for $1.5 \le x \le 3.0$; $r_{EC} = 100 - 13.333x$ for $3.0 \le x \le 4.5$; and $r_{EC} = 182.7 - 27.27x$ for $4.5 \le x \le 6.7$.[14] The remaining parameter ratings use the corresponding piecewise equations in the same published framework. Group sub-indices and weights used by the source program are summarized in Table 2.

$$I1 = r_{EC}; \; I2 = r_{(EC-SAR)}; \; I3 = (r_{SAR} + r_{Cl} + r_B)/3 \tag{2}$$

$$I4 = (1/N)\, \mathrm{sum}(r_{trace}); \; I5 = (r_{NO3-N} + r_{HCO3} + r_{pH})/3 \tag{3}$$

$$W_k = \frac{1/a_k}{\sum_h (1/a_h)} \tag{4}$$

The resulting weights were 0.4380, 0.2190, 0.1458, 0.1095, and 0.0870 for groups 1–5. Final aggregation followed the weighted-minimum operator proposed in the original method.[14] In compact form, using σ to order the five group weights in non-increasing order ($W\sigma[1] \ge W\sigma[2] \ge \ldots \ge W\sigma[5]$) and setting $W\sigma(6) = 0$, the operator is (**Equation 5**):

$$IWQI = \sum_{k=1}^{5} k\,[W_{\sigma(k)} - W_{\sigma(k+1)}] \min\{I_{\sigma(1)}, \ldots, I_{\sigma(k)}\}, \quad W_{\sigma(6)} = 0 \tag{5}$$

The suitability classes of the original IWQI method[14] are >80 suitable (S1), 60–80 moderately suitable (S2), 45–60 slightly suitable or marginally suitable (S3), 30–45 almost unsuitable (N1), and <30 unsuitable (N2). Because EC is an explicit IWQI component, EC–IWQI associations were treated as dependency diagnostics rather than as independent validation of the index.

Table 2. Structure of the Iraqi irrigation water quality index framework used by the source program[14-16]

Group	Parameters/representation	Weight	Sub-index construction
1. Salinity	EC	0.4380	I1 = rEC
2. Infiltration/permeability	EC–SAR combination	0.2190	I2 = rEC–SAR
3. Specific-ion toxicity	SAR, chloride, boron	0.1458	I3 = mean(rSAR, rCl, rB)
4. Trace-element toxicity	Available trace elements	0.1095	I4 = mean of available trace-element ratings
5. Miscellaneous effects	NO_3–N, HCO_3^-, pH	0.0870	I5 = mean(rNO_3–N, $rHCO_3$, rpH)

Note: Irrigation water quality index class boundaries: >80 suitable (S1); 60–80 moderately suitable (S2); 45–60 slightly suitable or marginally suitable (S3); 30–45 almost unsuitable (N1); <30 unsuitable (N2).
Abbreviations: EC: Electrical conductivity; SAR: Sodium adsorption rate.

2.4. Geospatial distance metric

Station spacing was derived directly from the updated WGS 84 coordinates. For each pair of successive monitoring stations, great-circle distance was calculated with the haversine relationship using Earth radius R = 6371.0088 km (**Equation 6**):

$$d_{ij} = 2R \arcsin\left(\sqrt{\sin^2\left(\frac{\phi_j - \phi_i}{2}\right) + \cos(\phi_i)\cos(\phi_j)\sin^2\left(\frac{\lambda_j - \lambda_i}{2}\right)}\right) \quad (6)$$

Cumulative monitoring-sequence distance for station *i* was the sum of all preceding inter-station segments. The resulting coordinate-based sequences were 897.48 km for the Tigris and 779.16 km for the Euphrates. These distances corrected the equal-spacing assumption inherent in normalized rank. They are deliberately described as cumulative inter-station geodesic distance rather than river network chainage because they connect station coordinates by successive great-circle segments and therefore do not represent channel meanders or hydraulic travel distance.

2.5. Landsat 8 vegetation-cover and optical-salinity mapping

Summer 2021 vegetation cover and surface salinity context was reconstructed from Landsat 8 OLI Collection 2 Level 2 surface reflectance in Google Earth Engine. Images from June 1 through August 31, 2021 were screened at the scene level with CLOUD_COVER < 20%. QA_PIXEL flags for fill, dilated cloud, cirrus, cloud, cloud shadow, and snow were removed, and QA_RADSAT was used to mask saturated pixels. Surface reflectance was scaled as surface reflectance (SR) = digital number (DN) × 0.0000275 − 0.2 before index calculation. Median summer composites were generated at the nominal 30-m Landsat resolution (**Equations 7–9**):

$$\text{NDVI} = (\text{NIR} - \text{RED}) / (\text{NIR} + \text{RED}) \quad (7)$$

$$\text{BSI} = [(\text{SWIR1} + \text{RED}) - (\text{NIR} + \text{BLUE})] / [(\text{SWIR1} + \text{RED}) + (\text{NIR} + \text{BLUE})] \quad (8)$$

$$\text{SI} = \text{sqrt}(\text{BLUE} \times \text{RED}) \quad (9)$$

To prevent invalid square-root products after Collection 2 offset scaling, SI was calculated only where both scaled BLUE and RED reflectances were non-negative; affected pixels were masked rather than transformed with an absolute-value operation. ESA WorldCover 2021 cropland provided the principal agricultural land-context layer. NDVI is interpreted as a spatial indicator of summer vegetation cover/greenness, whereas SI is an optical salinity indicator rather than field-measured soil EC. No station-level satellite regression or remote-sensing principal component analysis was used in the inferential hydrochemical results. This separation follows the calibration and transferability cautions emphasized in remote-sensing salinity research.[18-24]

2.6. Statistical analysis

Analyses were performed in Python 3.13 using statsmodels 0.14.6. Descriptive statistics included *n*, mean, standard deviation (SD), minimum, and maximum. The principal spatial predictor was cumulative monitoring-sequence geodesic distance, expressed per 100 km. Linear mixed-effects models were fitted by maximum likelihood with limited-memory Broyden–Fletcher–Goldfarb–Shanno optimization and station-specific random intercepts (**Equation 10**):

$$Y_{jk} = \beta_0 + \beta_1 D_j + \sum_m \beta_m \text{campaign}_{mk} + u_j + \varepsilon_{jk} \quad (10)$$

where D_j is cumulative monitoring-sequence geodesic distance in 100-km units, campaign is a fixed effect, u_j is the station-specific random intercept, and ε_{jk} is the within-station residual. March was selected as the reference campaign because it was the first 2021 campaign and provided complete EC/TDS coverage across both rivers. Separate models were fitted for EC, TDS, and IWQI within each river. For the combined analysis, the complete fixed-effects specification was response ~ river + distance + river × distance + campaign + river × campaign, with a station-specific random intercept; station identifiers are unique to, and therefore nested within, rivers. The river × distance term tests whether the slope per 100 km of cumulative monitoring-sequence geodesic distance differs between rivers. **Equation 10** and the combined-model specification are author-specified statistical models fitted to the present dataset; they are not empirical equations adopted from external sources. Effects are reported with two-sided 95% confidence intervals and *p*-values.

Robustness was evaluated through six complementary checks. First, Gaussian generalized estimating equations (GEE) with a first-order autoregressive (AR[1]) working correlation were fitted to each river–response combination. Second, each station was omitted in turn and the distance slope re-estimated. Third, April was removed entirely from the Euphrates analysis to test whether April missingness at Samawah, Nasiriyah, and Al-Madina altered the distance effect. Fourth, the valid-scale but discordant Al-Baghdadi April IWQI value (61.93) was excluded in a sensitivity analysis. Fifth, all Al-Madina observations were removed to test dependence on the March campaign maximum. EC–TDS and EC–IWQI dependency diagnostics were estimated with station-clustered Gaussian GEE adjusted for campaign. Finally, first-neighbor longitudinal autocorrelation was assessed for both station-averaged marginal residuals (fixed effects removed) and conditional residuals (fixed plus station random effects removed), using inverse-distance weights and 9,999 permutations.

Benjamini–Hochberg false-discovery rate adjustment was applied within each six-test residual family. Statistical significance was evaluated at α = 0.05.

3. Results

3.1. Dataset completeness and overall hydrochemical condition

The analysis retained 72 Tigris and 53 Euphrates EC/TDS observations, with 68 and 52 IWQI values, respectively. Tigris had a mean EC of 1.08 ± 0.65 dS/m and a mean TDS of 694.9 ± 420.6 mg/L. The Euphrates was more mineralized, with a mean EC of 1.55 ± 1.06 dS/m and a TDS of 1,008.7 ± 691.7 mg/L. Mean IWQI was 87.78 ± 8.60 in the Tigris and 82.53 ± 15.47 in the Euphrates (Table 3). The widest contrast in the minimum–maximum range was observed in the Euphrates, where EC ranged from 0.69 to 5.70 dS/m and IWQI from 45.13 to 95.62.

3.2. Coordinate-resolved electrical conductivity and total dissolved solids gradients

With unequal station spacing being properly accounted for, salinity gradients became noticeable in both rivers (Figures 2 and 3). In the Tigris, mixed-model EC increased by 0.217 dS/m per 100 km (95% confidence interval [CI]: 0.174–0.259; $p < 0.001$), and TDS increased by 140.7 mg/L per 100 km (95% CI: 112.7–168.7; $p < 0.001$) (Table 4). Across the 897.48-km monitoring sequence, these fixed-effect slopes correspond to model-estimated first-to-last changes of +1.94 dS/m and +1,263 mg/L. The main transition occurred downstream of the upper and middle low-salinity reaches, with a step increase around the Tharthar Arm/Baghdad sector and sustained high values from Ali Al-Gharbi through Al-Qurnah.

In the Euphrates, EC rose more rapidly, by 0.385 dS/m per 100 km (95% CI: 0.251–0.520; $p < 0.001$), while TDS rose by 254.4 mg/L per 100 km (95% CI: 170.6–338.3; $p < 0.001$) (Table 4). Across the 779.16-km sequence, the corresponding model-estimated changes were +3.00 dS/m and +1,983 mg/L. The lower-river transition was abrupt: March EC increased from 1.08 dS/m at Kifl to 2.70 dS/m at Shinafiyah, 2.90 dS/m at Samawah, 3.85 dS/m at Nasiriyah, and 5.70 dS/m at Al-Madina before decreasing to 3.10 dS/m at Al-Qurnah. June and July retained the same lower-river pattern at reduced magnitude, showing that the March maximum was superimposed on persistent downstream salinity.

3.3. River contrast and campaign effects

The combined model showed that the Euphrates deteriorated significantly faster with cumulative monitoring-sequence geodesic distance than the Tigris. The river × distance interaction was +0.169 dS/m per 100 km for EC ($p = 0.007$), +113.7 mg/L per 100 km for TDS ($p = 0.004$), and −2.81 IWQI units per 100 km ($p = 0.002$). These interactions directly test differences in the geodesic-distance deterioration rate rather than comparing river-specific slopes informally.

Campaign effects were smaller than the distance signal. With March as the reference, Euphrates EC was lower in June (−0.384 dS/m; $p = 0.004$) and July (−0.339 dS/m; $p =$

Table 3. Overall and campaign-specific EC, TDS, and IWQI statistics

River	Period	*n* EC	EC (dS/m)	TDS (mg/L)	*n* IWQI	IWQI
Tigris	Overall	72	1.08 ± 0.65	695 ± 421	68	87.78 ± 8.60
Tigris	March	18	1.09 ± 0.71	719 ± 471	18	87.16 ± 9.82
Tigris	April	18	1.12 ± 0.73	714 ± 464	18	86.44 ± 10.31
Tigris	June	18	1.02 ± 0.58	654 ± 386	16	89.70 ± 7.09
Tigris	July	18	1.09 ± 0.59	692 ± 388	16	88.04 ± 6.59
Euphrates	Overall	53	1.55 ± 1.06	1,009 ± 692	52	82.53 ± 15.47
Euphrates	March	14	1.89 ± 1.53	1,242 ± 995	14	78.57 ± 19.22
Euphrates	April	11	1.17 ± 0.56	743 ± 360	11	84.77 ± 12.63
Euphrates	June	14	1.50 ± 0.89	975 ± 577	14	84.33 ± 14.35
Euphrates	July	14	1.55 ± 0.92	1,018 ± 609	13	82.95 ± 15.29

Note: Values are provided as mean ± standard deviation.
Abbreviations: EC: Electrical conductivity; IWQI: Irrigation water quality index; TDS: Total dissolved solids.

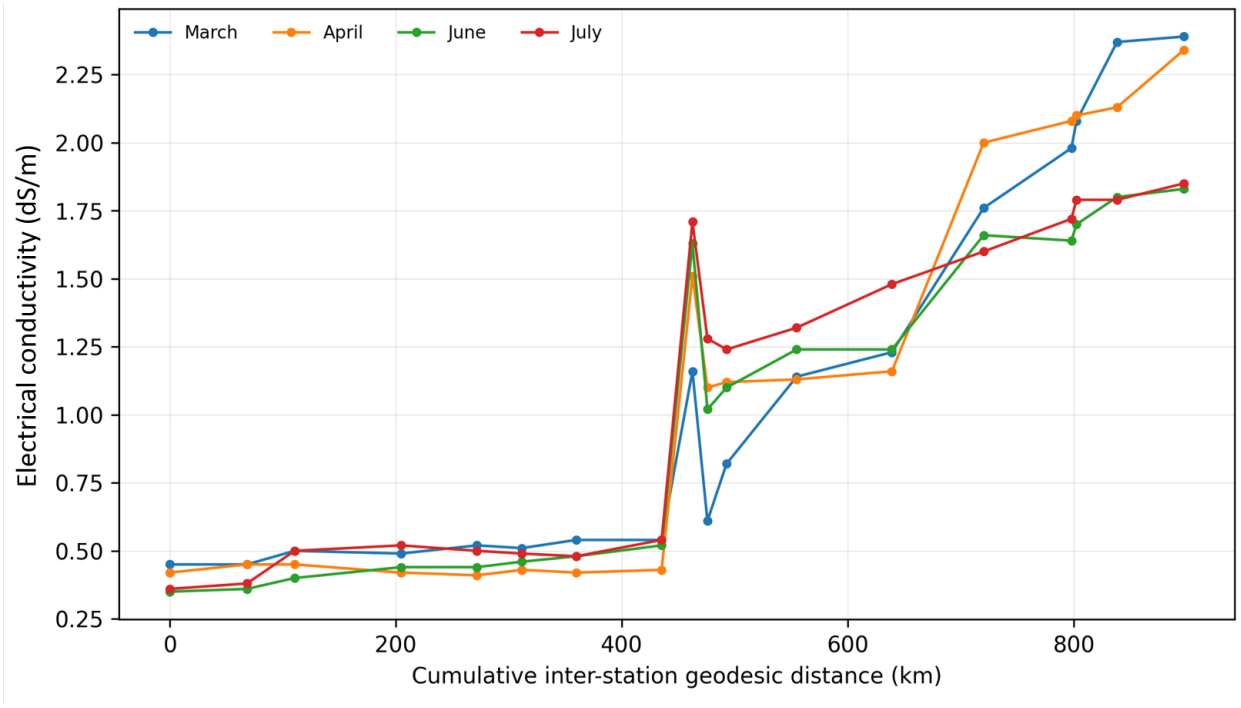


Figure 2. Tigris electrical conductivity profiles plotted against cumulative inter-station geodesic distance for the four 2021 campaigns. Distance is computed from the updated WGS 84 station coordinates.

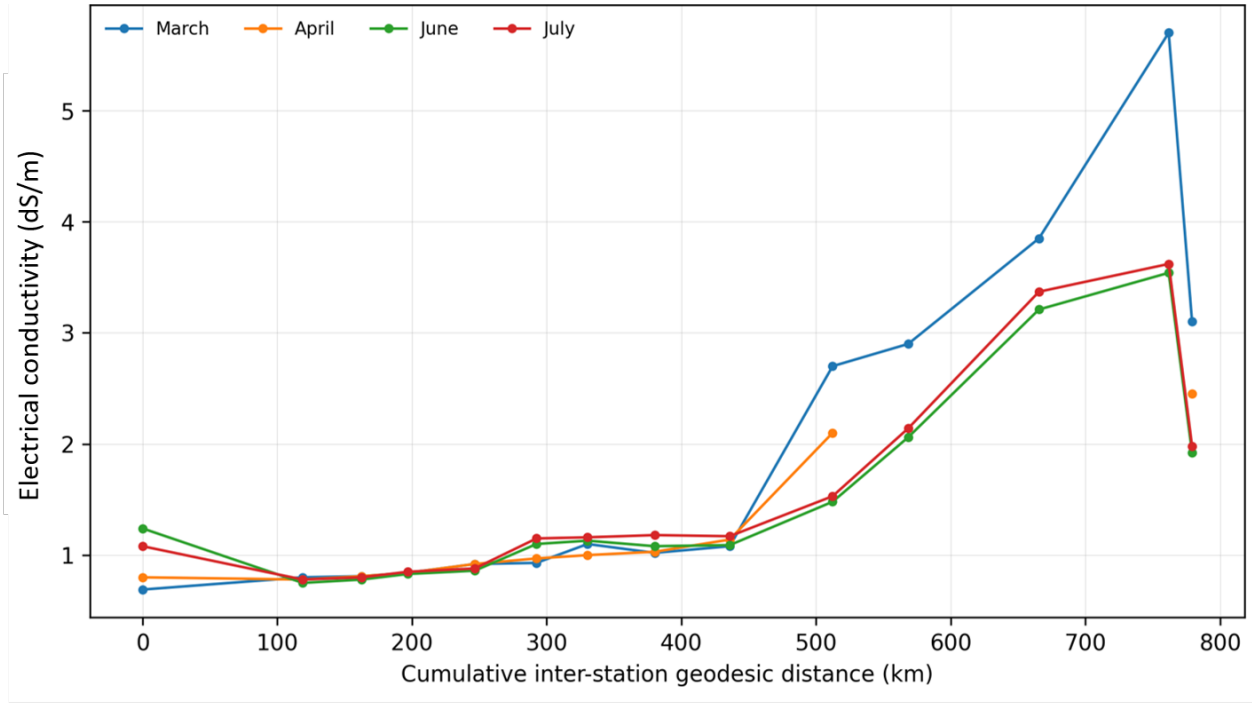


Figure 3. Euphrates electrical conductivity profiles plotted against cumulative inter-station geodesic distance for the four 2021 campaigns. April has no observations at Samawah, Nasiriyah, and Al-Madina.

Table 4. Distance-based mixed-effects estimates

River	Response	Slope/100 km	95% confidence interval	*p*	Sequence change	ICC
Tigris	EC (dS/m)	0.217	0.174 to 0.259	<0.001	+1.94 dS/m	0.66
Tigris	TDS (mg/L)	140.7	112.7 to 168.7	<0.001	+1,263 mg/L	0.68
Tigris	IWQI	−2.79	−3.33 to −2.26	<0.001	−25.07	0.59
Euphrates	EC (dS/m)	0.385	0.251 to 0.520	<0.001	+3.00 dS/m	0.72
Euphrates	TDS (mg/L)	254.4	170.6 to 338.3	<0.001	+1,983 mg/L	0.70
Euphrates	IWQI	−5.60	−7.61 to −3.59	<0.001	−43.64	0.66

Note: Slopes are per 100 km of cumulative inter-station geodesic distance. ICC is the station-level intraclass correlation estimated from the random-intercept model. River × distance interaction *p*-values in the combined model were 0.007 for EC, 0.004 for TDS, and 0.002 for IWQI.
Abbreviations: EC: Electrical conductivity; IWQI: Irrigation water quality index; TDS: Total dissolved solids.

0.012), while April showed a weaker contrast (−0.271 dS/m; $p = 0.065$). Because the three missing April observations occurred at the lower, more saline Euphrates stations, a dedicated analysis excluding April was performed. The Euphrates slopes remained 0.384 dS/m per 100 km for EC, 255.6 mg/L per 100 km for TDS, and −5.65 IWQI units per 100 km of cumulative monitoring-sequence geodesic distance (all $p < 0.001$); river × distance interactions also remained significant ($p = 0.005$, 0.003, and <0.001, respectively). Thus, the principal spatial inference does not depend on the incomplete April lower-river coverage.

3.4. Irrigation water quality index deterioration and classification

The irrigation water quality index decreased significantly with cumulative monitoring-sequence geodesic distance in both rivers (Figure 4). In the Tigris, the slope was −2.79 units per 100 km (95% CI: −3.33 to −2.26; $p < 0.001$), corresponding to a model-estimated decline of 25.07 units across the 897.48-km monitoring sequence. Upstream stations retained their >80 suitable (S1) status, while Ali Al-Gharbi, the Branching Regulators, Amarah Barrage, Qalat Saleh, and Al-Qurnah transitioned into the 60–80 moderately suitable (S2) category during the lower-river surveys.

In the Euphrates, IWQI declined by −5.60 units per 100 km of cumulative monitoring-sequence geodesic distance (95% CI: −7.61 to −3.59; $p < 0.001$), corresponding to a model-estimated decrease of 43.64 units across the 779.16-km monitoring sequence. The strongest deterioration began at Shinafiyah and continued through Samawah, Nasiriyah, and Al-Madina. In March, Al-Madina had the lowest IWQI score (45.13). Retaining the April Al-Baghdadi value of 61.93 in the primary analysis produced an isolated upper-river low but did not alter the pronounced lower-river gradient.

3.5. Dependency diagnostics and robustness

The expected EC–TDS relationship was estimated using station-clustered, campaign-adjusted GEE without assuming independence of repeated measures. TDS increased by 650.3 mg/L for each 1 dS/m increase in EC in the Tigris (95% CI: 643.5–657.0) and by 650.6 mg/L in the Euphrates (95% CI: 636.6–664.6; both $p < 0.001$). EC was inversely associated with IWQI: IWQI decreased by 12.65 units per 1 dS/m increase in EC in the Tigris (95% CI: −13.77 to −11.53) and by 13.73 units in the Euphrates (95% CI: −15.98 to −11.49; both $p < 0.001$).

The distance predictor remained stable under alternative covariance structures and data perturbations. Using GEE with an AR(1) working correlation, EC slopes were 0.216 and 0.403 dS/m per 100 km, and IWQI slopes were −2.74 and −5.70 units per 100 km for the Tigris and Euphrates, respectively (all $p < 0.001$) (Table 5). Leave-one-station-out slopes remained positive for EC (Tigris 95% CI: 0.212–0.232; Euphrates 95% CI: 0.309–0.443) and negative for IWQI (Tigris 95% CI: −3.02 to −2.67; Euphrates 95% CI: −6.42 to −4.81). Excluding the Al-Baghdadi April IWQI value strengthened, rather than weakened, the Euphrates IWQI slope to −5.76 units per 100 km (95% CI: −7.67 to −3.86; $p < 0.001$). Removing Al-Madina still yielded significant Euphrates gradients for EC (+0.309 dS/m per 100 km), TDS (+207.6 mg/L per 100 km), and IWQI (−4.81 units per 100 km; all $p < 0.001$).

First-neighbor Moran tests provided no evidence of residual longitudinal autocorrelation under either residual

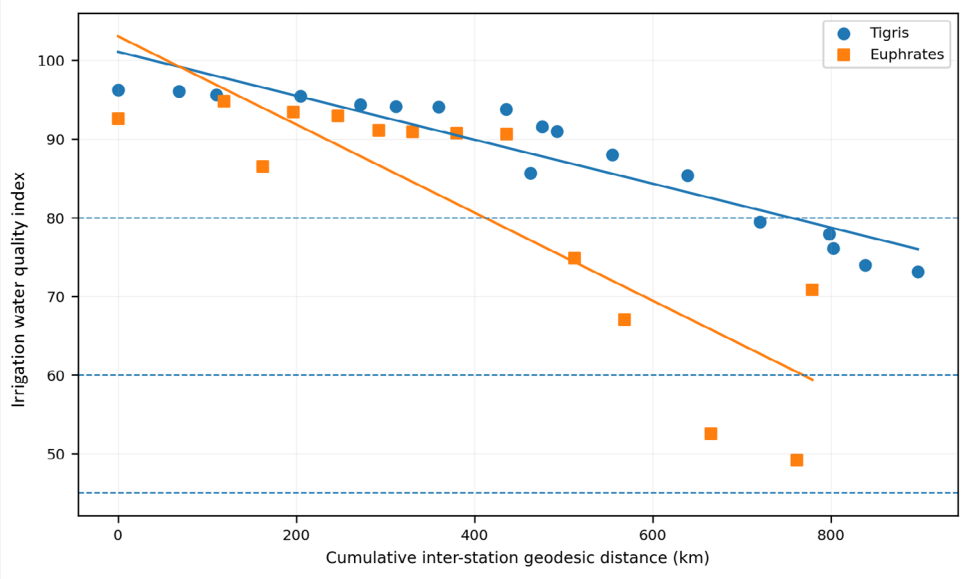


Figure 4. Station-mean irrigation water quality index (IWQI) versus cumulative inter-station geodesic distance. Solid lines are river-specific fixed-effect trends averaged across the four campaign effects; dashed horizontal lines mark the principal operational IWQI class boundaries.

definition after false-discovery rate control. For station-averaged marginal residuals, raw permutation p-values ranged from 0.273 to 0.935 and adjusted q values from 0.817 to 0.935. For conditional residuals, raw p-values ranged from 0.248 to 0.935, and all adjusted q values were 0.935. The agreement between marginal and conditional diagnostics indicates that the absence of residual spatial structure is not an artifact of subtracting the station random intercept.

3.6. Basin-scale vegetation-cover and optical-salinity patterns

The June–August Landsat composite showed clear basin-scale spatial variation in vegetation cover. Higher NDVI values occurred in northern Iraq and in several irrigated river-associated areas, whereas lower NDVI values were widespread across central and southern areas. The optical SI also showed broad spatial contrasts, with higher values across parts of central and southern Iraq (Figure 5). Because SI was not calibrated against field soil electrical conductivity, these values are interpreted only as optical surface patterns and not as quantitative evidence of soil salinity. Neither map was used to infer river EC or to attribute vegetation condition directly to river-water salinity.

4. Discussion

4.1. A geodesic-distance-resolved downstream salinity gradient

The principal result is a strong increase in dissolved salts along cumulative monitoring-sequence geodesic distance in both Iraqi rivers. Replacing normalized station order with cumulative great-circle distances between successive WGS 84 station coordinates removes the assumption of equal station spacing, but still does not represent river-channel chainage or hydraulic travel distance. EC increased by 0.217 dS/m per 100 km in the Tigris and by 0.385 dS/m per 100 km in the Euphrates. The significant river × distance interactions for EC, TDS, and IWQI show that the steeper deterioration in the Euphrates is not explained simply by its monitoring-sequence length.

This result is consistent with recent Iraqi evidence but adds a common inferential scale. Oleiwi and Al-Dabbas[8] documented Tigris discharge, salinity, and dissolved-load variation from Mosul to Baghdad, while Al-Sekar and Al-Dabbas[9] linked lower-Tigris hydrochemistry to discharge variation. Euphrates studies have repeatedly identified greater downstream mineralization from central toward southern Iraq.[10,11] The present analysis extends those observations by estimating river-specific salinity rates per 100 km under a repeated-measures model and by demonstrating that the result persists under AR(1) correlation and station-deletion sensitivity.

4.2. The lower Euphrates as the critical transition reach

The Euphrates shows the largest change after Kifl, with a marked transition through Shinafiyah, Samawah, Nasiriyah, and Al-Madina. The March value of 5.70 dS/m

Table 5. Robustness analyses for the distance-based inference

Analysis	River/response	Estimate	95% CI or range	Inference
AR(1) GEE	Tigris EC	0.216/100 km	0.182 to 0.249	$p < 0.001$
AR(1) GEE	Euphrates EC	0.403/100 km	0.226 to 0.581	$p < 0.001$
AR(1) GEE	Tigris IWQI	−2.74/100 km	−3.25 to −2.24	$p < 0.001$
AR(1) GEE	Euphrates IWQI	−5.70/100 km	−7.93 to −3.47	$p < 0.001$
Leave-one-station-out	Tigris EC/IWQI	All slopes preserved	EC: 0.212–0.232; IWQI: −3.02 to −2.67	18/18 fits
Leave-one-station-out	Euphrates EC/IWQI	All slopes preserved	EC: 0.309–0.443; IWQI: −6.42 to −4.81	14/14 fits
Exclude April	Euphrates EC	0.384/100 km	0.247 to 0.521	$p < 0.001$
Exclude April	Euphrates IWQI	−5.65/100 km	−7.58 to −3.72	$p < 0.001$
Exclude Al-Baghdadi 61.93	Euphrates IWQI	−5.76/100 km	−7.67 to −3.86	$p < 0.001$
Exclude Al-Madina	Euphrates EC	0.309/100 km	0.192 to 0.426	$p < 0.001$
Exclude Al-Madina	Euphrates IWQI	−4.81/100 km	−6.89 to −2.74	$p < 0.001$
Marginal residual Moran + FDR	All 6 models	No residual signal	$q = 0.817–0.935$	Not significant
Conditional residual Moran + FDR	All 6 models	No residual signal	$q = 0.935$ for all	Not significant

Abbreviations: AR(1): First-order autoregressive correlation; CI: Confidence interval; EC: Electrical conductivity; FDR: False-discovery rate; IWQI: Irrigation water quality index; TDS: Total dissolved solids.

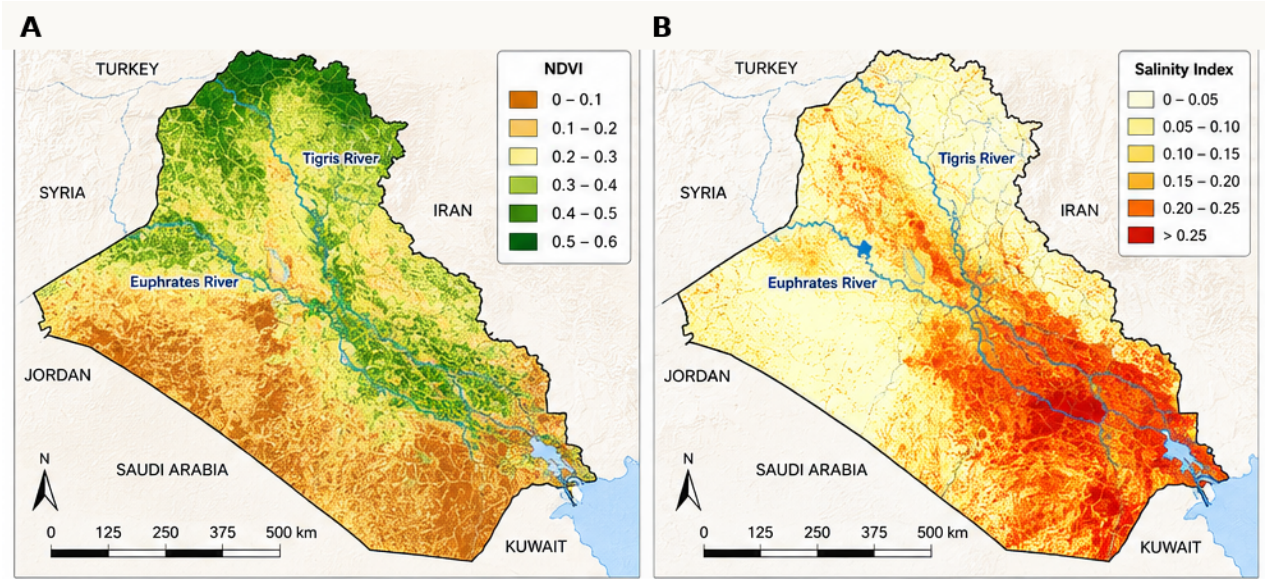


Figure 5. Landsat 8 summer 2021 spatial patterns of (A) Normalized difference vegetation index (NDVI)-derived vegetation cover/greenness and (B) optical salinity index (SI) across Iraq. SI is not field-calibrated soil electrical conductivity, and neither map is used as a direct predictor of river-water chemistry.

at Al-Madina is the highest observation among the four campaigns, but it does not create the downstream signal by itself: removing Al-Madina reduces the EC slope from 0.385 to 0.309 dS/m per 100 km, yet the gradient remains highly significant. This sensitivity result is important because it separates a conspicuous campaign maximum from the underlying lower-river salinity structure.

Several processes may contribute to this trend, including reduced dilution, evaporation, agricultural return flow, municipal inputs, and interactions with saline groundwater and drainage systems.[10,13,25,26] The present design cannot assign quantitative contributions to these processes because synchronized discharge data and source tracing were unavailable. The supported inference is therefore spatial and hydrochemical: the lower Euphrates was more saline and deteriorated more rapidly along the monitored cumulative geodesic-distance sequence.

4.3. Irrigation suitability and mathematical dependence within irrigation water quality index

The IWQI analysis expresses salinity deterioration in terms of irrigation suitability. The downstream IWQI gradient was approximately twice as steep in the Euphrates as in the Tigris per 100 km of cumulative monitoring-sequence geodesic distance. This pattern is consistent with the Iraqi IWQI literature, which reports generally suitable upstream water and progressive deterioration toward the south.[14,15] The valid-range Al-Baghdadi April value was retained in the primary dataset, and its exclusion did not alter the inference. Because EC contributes directly to IWQI, the EC–IWQI relationship is partly mathematical; the cluster-based EC–IWQI analysis was therefore used only to describe dependency within the archived index.

From an irrigation-management perspective, the results support reach-specific monitoring rather than direct intervention prescriptions. A global 2026 meta-analysis showed that irrigation with saline water can increase soil salinity and reduce crop yield, with effects depending on water salinity, climate, irrigation amount, soil properties, and crop type.[27] Recent work in the Badra agricultural region of Iraq similarly identified EC and TDS as important constraints on irrigation-water suitability.[28] Decisions on crop selection, leaching, blending, or irrigation scheduling would require additional information on discharge, field soil salinity, crop sensitivity, groundwater, drainage, and irrigation practices.

4.4. Hydrochemical context relative to recent Iraqi studies

The observed EC and TDS gradients are consistent with, but extend, recent hydrochemical studies from Iraq. Long-term work on the Tigris in Baghdad by Nassrullah *et al.*[12] considered a broader suite of physicochemical variables and identified both natural and anthropogenic influences. Awadh *et al.*[13] combined hydrochemistry and isotopes to examine river–aquifer interactions in the western Euphrates. The Tarmiah groundwater study[29] further shows that irrigation suitability can differ between local groundwater and surface-water settings. The present study adds a repeated, coordinate-resolved comparison of the two major rivers rather than attempting ionic-facies or source-apportionment analysis.

The reported Ca^{2+} and Na^{+} ranges provide supporting hydrochemical context for the downstream mineralization pattern. Sodium reached 760 mg/L in the lower Euphrates in March, while the corresponding Tigris maxima were lower. Calcium also increased downstream in both systems. Together with measured TDS, these observations are consistent with increasing dissolved ion content. Because the cation record was less complete across station–campaign combinations than EC/TDS/IWQI, it is interpreted as supporting evidence rather than as a repeated-measures response.

4.5. Vegetation cover and geospatial interpretation

Geospatial data serve two intentionally distinct purposes. First, station coordinates define the distance metric used in the river models. Second, Landsat NDVI independently describes summer vegetation-cover patterns, while SI provides optical surface context. Remote sensing can characterize vegetation condition and salinity-related surface spectral patterns,[18-23] but optical pixels cannot infer river-water chemistry without appropriate calibration and validation. A 2026 systematic review of water-quality indices and remote-sensing models highlighted persistent challenges in preprocessing, uncertainty analysis, and transferability.[24] Accordingly, the Landsat component provided spatial context and was not used to generate unsupported EC–NDVI or EC–SI predictions.

4.6. Monitoring and water-management implications

Distance-resolved gradients provide practical guidance for monitoring. In the Tigris, more intensive surveillance is supported from Kut southward to Ali Al-Gharbi. In the Euphrates, Shinafiyah marks the principal transition, and the reach through Samawah, Nasiriyah, and Al-Madina warrants more frequent salinity and ionic monitoring. Combining continuous or high-frequency EC/TDS measurements with periodic full-ion analyses, discharge observations, and field soil EC measurements would help future monitoring distinguish concentration changes related to dilution from those associated with return flows

or other inputs.

Such a monitoring strategy aligns with broader frameworks of water resilience, which recommend integrated technological, environmental, and institutional approaches.[30] Digitalizing monitoring facilities can support the continuity and availability of environmental information; nevertheless, digitalization itself does not eliminate governance and allocation problems.[31] Equally important is effective communication of monitoring information among different agencies and water users; communicative rationality theory provides a general rationale for stakeholder engagement based on transparency and an evidence base.[32] Finally, at the farm scale, some experiments in Iraq show that irrigation scheduling and field management can make a difference in semi-arid conditions.[33]

4.7. Scope of inference

This study covered four coordinated campaigns in 2021 and therefore compared within-year campaigns rather than providing a full annual climatology or an interannual trend. Cumulative monitoring-sequence geodesic distance accounts for unequal spacing among monitoring locations but is neither river-channel chainage nor hydraulic travel distance; all per-100-km coefficients refer specifically to the geodesic-distance metric defined by the sequence of WGS 84 station coordinates. Discharge was not available as a station-by-campaign covariate, so the models estimated spatial gradients without a discharge-response term. Archived IWQI values were analyzed using the methodology described above; the valid-range Al-Baghdadi score was retained in the primary analysis and excluded only in sensitivity testing. Landsat NDVI represented summer vegetation cover/greenness, while SI remained an uncalibrated optical surface index rather than a measurement of soil salinity.

5. Conclusion

Using WGS 84 station coordinates and accounting explicitly for unequal station spacing resolved a consistent downstream salinity gradient in the Iraqi Tigris–Euphrates monitoring network. Across 897.48 km of cumulative monitoring-sequence geodesic distance in the Tigris, EC increased by 0.217 dS/m per 100 km, and IWQI declined by 2.79 units per 100 km. Across 779.16 km of the same metric in the Euphrates, the corresponding changes were 0.385 dS/m and −5.60 IWQI units per 100 km. The Euphrates deterioration rate was significantly steeper for EC, TDS, and IWQI, with the principal transition beginning at Shinafiyah and intensifying through Samawah, Nasiriyah, and Al-Madina. These inferences persisted under AR(1) GEE, leave-one-station-out analysis, exclusion of April, sensitivity to the Al-Baghdadi IWQI value, removal of Al-Madina, and both marginal- and conditional-residual spatial-autocorrelation tests.

Landsat NDVI resolved a basin-scale summer vegetation-cover pattern, with greener northern and irrigated river-associated landscapes and lower vegetation cover across broad central and southern areas. The SI layer is interpreted only as an uncalibrated optical surface pattern; it is not treated as a soil-salinity measurement or as a predictor of river chemistry. For management, the results support intensified salinity surveillance in the lower Tigris and especially the middle-to-lower Euphrates. More specific irrigation interventions require additional discharge, full-ion chemistry, river-channel chainage, field soil EC, groundwater, drainage, crop sensitivity, and irrigation-practice data. The coordinate-resolved framework can be repeated in subsequent monitoring years to test whether salinity transition zones and associated vegetation-cover patterns shift as basin water availability changes.

Acknowledgments

None.

Funding

None.

Conflict of interest

The authors declare no financial or non-financial competing interests related to this manuscript.

Author contributions

Conceptualization: Raghad Mouhamad, Afrah L. Mohammed Rasheed
Formal analysis: Raghad Mouhamad
Investigation: Afrah L. Mohammed Rasheed, Khanssaa M. Abdulmajed, Shrooq R. Hameed
Methodology: Raghad Mouhamad, Afrah L. Mohammed Rasheed
Writing–original draft: Afrah L. Mohammed Rasheed, Raghad Mouhamad
Writing–review & editing: Raghad Mouhamad, Khanssaa M. Abdulmajed, Shrooq R. Hameed

Availability of data

The complete quality-controlled station–campaign EC/TDS/IWQI matrix, analysis code, and data supporting the findings of this study are available from the corresponding author upon reasonable request.

References

1. Zlati ML, Antohi VM, Ionescu RV, Iticescu C, Georgescu LP. Quantifying the impact of the water security index on socio-economic development in EU27. *Socioecon Plann Sci*. 2024;93:101912.

doi: 10.1016/j.seps.2024.101912

2. Darvishi BA, Papi R, Soleimani M, Neysani Samani N, *et al*. Human interventions and climate change trigger water crisis in the Tigris and Euphrates Basin. *Environ Sci Policy*. 2026;177:104300.

doi: 10.1016/j.envsci.2025.104300

3. Haghighi AT, Akbari M, Noori R, *et al*. The impact of Turkey's water resources development on the flow regime of the Tigris River in Iraq. *J Hydrol Reg Stud*. 2023;48:101454.

doi: 10.1016/j.ejrh.2023.101454

4. Delavar M, Kuchak VS, Morid S, Zaghiyan MR, Babbaeian F. Country-base analyses of agriculture water consumption in the Tigris-Euphrates basin using modified SWAT model and water accounting plus framework. *Agric Water Manag*. 2026;332:110465.

doi: 10.1016/j.agwat.2026.110465

5. Luan W, Li X, Kuang W, *et al*. Quantitative assessment of the water stress in the Tigris-Euphrates River Basin driven by anthropogenic impacts. *Remote Sens*. 2025;17(4):662.

doi: 10.3390/rs17040662

6. Al-Ansari N, Ali A, Knutsson S. Present conditions and future challenges of water resources problems in Iraq. *J Water Resour Prot*. 2014;6(12):1066-1098.

doi: 10.4236/jwarp.2014.612102

7. Al-Ansari N. Hydro-politics of the Tigris and Euphrates Basins. *Engineering*. 2016;8(3):140-172.

doi: 10.4236/eng.2016.83015

8. Oleiwi AS, Al-Dabbas M. The parameters discharge, salinity and dissolved loads of Tigris River from Mosul to Baghdad, Iraq. *Iraqi J Sci*. 2024;65(6):3176-3194.

doi: 10.24996/ijs.2024.65.6.19

9. Al-Sekar H, Al-Dabbas M. The influence of the Tigris River discharge on the hydrochemistry with time, from Baghdad to Amara, Southern Iraq. *Iraqi Geol J*. 2022;55(2D):140-156.

doi: 10.46717/igj.55.2d.12ms-2022-10-28

10. Muhammed M, Al-Dabbas M. Impact of climatic change and shortage of water flow on the Euphrates River water salinity between Al-Hindyia and Al-Nasiriya, Southern Iraq. *Iraqi Geol J*. 2022;55(2A):139-152.

doi: 10.46717/igj.55.2a.10ms-2022-07-26

11. Seeyan S, Mahdi K, Diwan T, *et al*. Hydrochemical assessment and spatiotemporal variations for water quality in the Euphrates River in the western, central and southern of Iraq. *Environ Earth Sci*. 2026;85(6):151.

doi: 10.1007/s12665-026-12887-4

12. Nassrullah SA, Saihood SK, Mahmood W, Ismail AH, Farhan AA, Hussein FM. Water quality and hydrochemistry of Tigris River in a metropolitan city: long-term assessment. *Case Stud Chem Environ Eng*. 2026;13:101375.

doi: 10.1016/j.cscee.2026.101375

13. Awadh SM, Al-Kubaisi MHD, Anees MT, Abu Bakar AF, Bin Arif MR. Transboundary hydrogeology and controlling factors of Euphrates water chemistry: Insights from hydrochemistry, stable isotopes, and residence times in Syria and Western Iraq. *Environ Earth Sci*. 2026;85(9):335.

doi: 10.1007/s12665-026-12922-4

14. Al-Meini AJK. A proposed index of water quality assessment for irrigation. *Eng Technol J*. 2010;28(22):6557-6579.

doi: 10.30684/etj.28.22.9

15. Saloom HS, Oleiwi IAM. Evaluation of irrigation water quality index (IWQI) for main Iraqi rivers (Tigris, Euphrates, Shatt Al-Arab and Diyala). *Iraqi J Agric Sci*. 2017;48(4):1010-1020.

doi: 10.36103/ijas.v48i4.358

16. Ayers RS, Westcot DW. *Water Quality for Agriculture*. FAO Irrigation and Drainage Paper 29 Rev. 1. Rome, Italy: Food and Agriculture Organization of the United Nations; 1994.

17. Iticescu C, Murariu G, Georgescu LP, Burada A, Topa CM. Seasonal variation of the physico-chemical parameters and water quality index (WQI) of Danube water in the transboundary Lower Danube area. *Rev Chim*. 2016;67(9):1843-1849.

18. Metternicht G, Zinck JA. Remote sensing of soil salinity: potentials and constraints. *Remote Sens Environ*. 2003;85(1):1-20.

doi: 10.1016/S0034-4257(02)00188-8

19. Corwin DL, Scudiero E. Review of soil salinity assessment for agriculture across multiple scales using proximal and/or remote sensors. In: *Advances in Agronomy*. Vol 158. Amsterdam, Netherlands: Elsevier; 2019:1-130.

doi: 10.1016/bs.agron.2019.07.001

20. Allbed A, Kumar L, Aldakheel YY. Assessing soil salinity using soil salinity and vegetation indices derived from IKONOS high-spatial resolution imageries: applications in a date palm dominated region. *Geoderma*. 2014;230-231:1-8.

doi: 10.1016/j.geoderma.2014.03.025

21. Scudiero E, Skaggs TH, Corwin DL. Regional-scale soil salinity assessment using Landsat ETM+ canopy reflectance. *Remote Sens Environ*. 2015;169:335-343.

doi: 10.1016/j.rse.2015.08.026

22. Sahbeni G, Ngabire M, Musyimi PK, Szekely B. Challenges and opportunities in remote sensing for soil salinization mapping and monitoring: a review. *Remote Sens*. 2023;15(10):2540.

doi: 10.3390/rs15102540

23. Wang F, Han L, Liu L, *et al*. Advancements and perspective in the quantitative assessment of soil salinity utilizing remote sensing and machine learning algorithms: a review. *Remote Sens*. 2024;16(24):4812.

doi: 10.3390/rs16244812

24. Amin G, Pourret O, Dupin V, Guérin-Rechdaoui S, Dujany A. Comparing AI-driven approaches for predicting river water quality: a systematic review of water quality indices and remote sensing methods. *Water Res*. 2026;301:126047.

doi: 10.1016/j.watres.2026.126047

25. Montazeri A, Mazaheri M, Morid S, Mosaddeghi M. Effects of upstream activities of Tigris-Euphrates River Basin on water and soil resources of Shatt al-Arab Border River. *Sci Total Environ*. 2023;858:159751.

doi: 10.1016/j.scitotenv.2022.159751

26. Olson KR, Speidel DR. Tigris, Euphrates, and Shatt Al-Arab River system: historic and modern attempts to manage and restore Iraq's lifeline. *Open J Soil Sci*. 2024;14(1):28-63.

doi: 10.4236/ojss.2024.141003

27. Qiao X, Hao Z, Liu H, Liu Y. A global meta-analysis of the effects of irrigation with water containing salts on saline-alkali soils. *Agric Water Manag*. 2026;325:110202.

doi: 10.1016/j.agwat.2026.110202

28. Al Gburi HF, Al Ali IA, Majeed AH, Mouhamad R. Groundwater quality assessment for irrigation purposes: case study Badra Region, North East Wasit Governorate, southeast of Iraq. *Asian J Water Environ Pollut*. 2026;23(4):026140096.

doi: 10.36922/AJWEP026140096

29. Ismail AH, Ghanim H, Sarhan AH. Hydrochemistry of shallow groundwater and its assessment for drinking and irrigation purposes in Tarmiah district, Baghdad governorate, Iraq. *Groundw Sustain Dev*. 2020;10:100300.

doi: 10.1016/j.gsd.2019.100300

30. Hasan N, Pushpalatha R, Roshni T, Sruthy S. State of the art review of recent trends and challenges and future directions in building water resilience. *Discov Sustain*. Published online 2026.

doi: 10.1007/s43621-026-04222-5

31. Antohi VM, Barbuta-Misu N, Georgescu PL, Zlati ML, Fortea C. Digital transformation, innovation, and green transitions: A panel data analysis of structural drivers in the European economy. *Green Finance*. 2026;8(3):468-500.

doi: 10.3934/gf.2026017

32. Camli AY, Virlanuta FO, Palamutcuoglu BT, Barbuta-Misu N, Guler S, Zungun D. A study on developing a communicative rational action scale. *Sustainability*. 2021;13(11):6317.

doi: 10.3390/su13116317

33. Atiyah AH, Ati AS, AL-Halfi KM, Dawod SS, Mouhamad RS. Integrated effects of controlled traffic farming and irrigation scheduling on water productivity and yield of pumpkin under semi-arid sprinkler irrigation. *Asian J Water Environ Pollut*. 2026;23(4):026200145.

doi: 10.36922/AJWEP026200145